JPE 16-5-32

http://dx.doi.org/10.6113/JPE.2016.16.5.1939
ISSN(Print): 1598-2092 / ISSN(Online): 2093-4718

First-order Generalized Integrator Based Frequency Locked Loop and Synchronization for Three-Phase Grid-connected Converters under Adverse Grid Conditions

Zhaoxu Luo*, Mei Su*, Yao Sun†, Zhangjie Liu*, and Mi Dong*

*,†School of Information Science and Engineering, Central South University, Changsha, China

Abstract

This paper presents an alternative frequency adaptive grid synchronization technique named HDN-FLL, which can accurately extract the fundamental positive- and negative-sequence components and interested harmonics in adverse three-phase grid voltage. The HDN-FLL is based on the harmonic decoupling network (HDN) consisting of multiple first order complex vector filters (FOCVF) with a frequency-locked loop (FLL), which makes the system frequency adaptive. The stability of the proposed FLL is strictly verified to be global asymptotically stable. In addition, the linearization and parameters tuning of the FLL is also discussed. The structure of the HDN has been widely used as a prefilter in grid synchronization techniques. However, the stability of the general HDN is seldom discussed. In this paper, the transfer function expression of the general HDN is deduced and its stability is verified by the root locus method. To show the advantages of the HDN-FLL, a simulation comparison with other gird synchronization methods is carried out. Experimental results verify the excellent performance of the proposed synchronization method.

Key words: First-order generalized integrator, Frequency-locked loop, Grid-connected converter, Grid synchronization, Harmonic detection

I. INTRODUCTION

Nowadays, more and more renewable energy-based distributed generation (DG) systems are being connected to utility grids through grid-interfaced converters [1]-[4], such as wind turbine generator systems (WTGS), solar energy generating systems (SEGS), etc. They are expected to be an effective solution to help ease the cost of energy, energy security and relevant environmental issues introduced by conventional large centralized power generators.

On the other hand, the grid-interfaced converters used in DG systems should be carefully controlled to meet the strict grid codes [6], [7]. For instance, in many countries a WTGS needs to be on grid and to provide reactive power to support the grid voltage even under grid fault conditions. WTGSs are only allowed to be disconnected from the grid when the grid voltage drops below a lower limit protection value, which means that a WTGS must has the ability of fault ride-through. To that end, one of the most important aspects to be considered in the control of these power converters is fast and exact synchronization with grid voltages at the point of common coupling (PCC), even if the grid voltage is unbalanced and severely distorted.

To synchronize with grid voltage, the magnitude, phase angle and frequency of the fundamental positive-sequence component (FPC) need to be known. A phase-locked loop (PLL) based on the synchronous reference frame (SRF-PLL) is the most widely used synchronization technique for three-phase power systems. The SRF-PLL shows fast and accurate performance under ideal grid conditions. However, its performance is significantly degraded if the grid voltage condition gets worse, since it is quite sensitive to voltage imbalance and harmonic distortion.

Manuscript received Dec. 27, 2015; accepted May 16, 2016
Recommended for publication by Associate Editor Kyo-Beum Lee.
†Corresponding Author: yaosun@gmail.com
Tel: +86-0731-8876070, Central South University
*School of Information Science & Eng., Central South Univ., China

Different advanced synchronization methods have been proposed to improve the performance of the SRF-PLL under adverse gird conditions. Most of these methods employ prefilters or a decoupling network to extract the FPC from the grid voltage and to feed it to the SRF-PLL. The Decoupled Double SRF-PLL (DDSRF-PLL) presented in [9] uses a decoupling network to separate the FPC and the fundamental negative-sequence component (FNC). Another synchronization technique called 'Dual Second Order Generalized Integrator PLL' can detect the FPC of the utility voltage under unbalanced and distorted conditions [10]. However, these two methods are incapable of detecting harmonics, which can be useful for harmonic compensation in some cases [8]. In [11]-[15], PLL techniques based on the harmonic decoupling network (HDN) are proposed. Due to the characteristic of the HDN, all of the desired frequency components (even harmonics) are allowed to be extracted from non-ideal grid voltages. However, the stability of the HDN is seldom discussed. There are other PLL-based synchronization techniques suitable for operating under adverse grid conditions [16]-[20], such as the Cascaded DSC PLL (CDSC-PLL) [16], a PLL method using the fast Fourier transform (FFT) concept (FFT-PLL) [17], a PLL based on an adaptive low-pass notch filter (LPN-PLL) [18], etc, which have been shown to have excellent performance in some way.

A type of grid synchronization technology using the concept of the frequency-locking loop (FLL) instead of the PLL has been studied as well. Compared with the PLL-type ones, synchronization technologies of the FLL-type are more suitable for grid conditions which experiences phase-angle jumps, because FLL estimation of the grid frequency does not experience such sudden changes [11]. Many literatures have presented methods based on the concept of the FLL [11], [13], [23]-[24]. For instance, [11] presents a technique called MSOGI-FLL, which uses a second-order generalized integrator based FLL to make the system frequency adaptive. Although these methods have been shown to have good performance under adverse grid conditions, their computation is a bit complicated.

This paper proposes a FLL-type synchronization technology, i.e., the HDN-FLL, for the grid-interfaced converters in three-phase DG systems. The HDN-FLL is based on a harmonic decoupling network consisting of multiple first order complex vector filters (FOCVF) with a FLL, which makes the system frequency adaptive. Significantly, the stability of the proposed FLL and HDN structure are verified.

This paper is organized as follows. Section II presents a stability analysis and parameters tuning for the proposed FLL. In Section III, the stability of the HDN is verified, and the HDN-FLL is presented. Section IV presents simulation results and performance comparisons between the HDN-FLL and other synchronization technologies. In Section V, the performance of the HDN-FLL is evaluated by experimental results. Section VI provides some conclusions.

II. FLL

A. First Order Generalized Integrator

The generalized integrator (GI) originates from the principle that the time-domain convolution product of a sinusoidal function by itself gives rise to a sinusoidal term multiplied by a time variable. GIs have been widely used in applications associated with sinusoidal signals, like frequency detecting, harmonics notch filters, static error free tracking, etc. The second order generalized integrator (SOGI) for single phase sinusoidal signals has been discussed in many literatures [21]-[24].

Considering the case of the GI for three-phase sinusoidal voltage signals, the GI is supposed to make the following equation true:

$$\boldsymbol{v} * GI(t) = \boldsymbol{v} \cdot t \tag{1}$$

where the symbol $*$ represents the convolution operation, and $\boldsymbol{v}$ is a three-phase sinusoidal voltage signal, which can be described in term of a vector as:

$$\boldsymbol{v} = v_\alpha + jv_\beta = A\cos(\omega t + \varphi) + jA\sin(\omega t + \varphi) \tag{2}$$

By applying Laplace transforms to (1), the generalized integrator in the Laplace domain can be obtained as:

$$\mathrm{FOGI}(s) = \frac{L[\boldsymbol{v} \cdot t]}{L[\boldsymbol{v}]} = \frac{s}{s^2 + \omega^2} + j\frac{\omega}{s^2 + \omega^2} = \frac{1}{s - j\omega} \tag{3}$$

where the resonator $1/(s - j\omega)$ is the desired first-order generalized integrator (FOGI) for three-phase sinusoidal signals. Moreover, (3) indicates that the FOGI can be seen as the sum of two SOGIs at the real axis and the imaginary axis, respectively.

B. FOCVF

SOGI based filters have been used to filter gird voltages and to extract harmonics. However, they do not have the ability to make a distinction between positive- and negative-sequences at the same frequency. Thus, a positive-/negative-sequence calculation (PNSC) block is needed to do this job.

To distinguish between the positive- and negative-sequence directly, a first order complex vector filter based on the FOGI has been developed, whose structure is shown in Fig. 1.

According to Fig. 1(a), the transfer function of the FOCVF can be derived as:

$$CV(s) = \frac{\omega_c \mathrm{FOGI}(s)}{1 + \omega_c \mathrm{FOGI}(s)} = \frac{\omega_c}{s - j\omega' + \omega_c} \tag{4}$$

where ω' is the center frequency of the FOCVF (it is also the resonance frequency of the FOGI); ω_c is the cutoff frequency, and $\omega_c > 0$. It can be concluded that the bandwidth and steady-state gain of (4) depend only on the

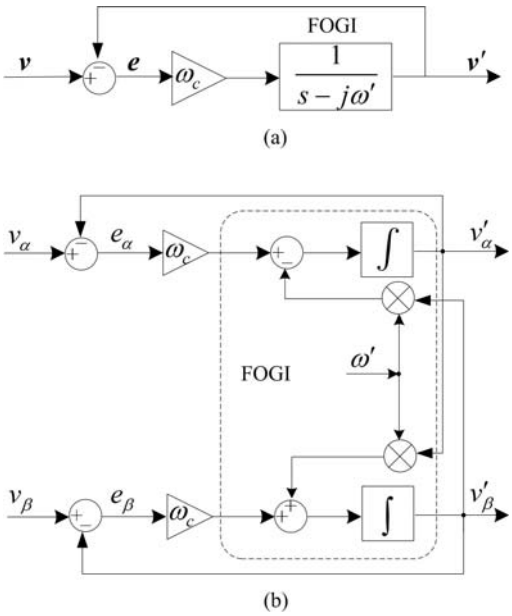

Fig. 1. Structure of FOCVF ((a) in the vector form and (b) in the scalar form).

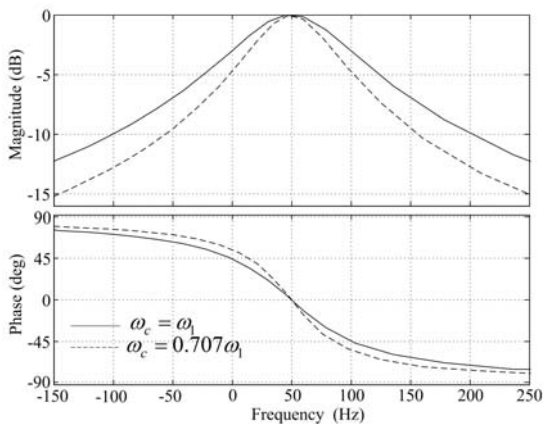

Fig. 2. Bode diagram of FOCVF when $\omega' = 100\pi$.

cutoff frequency ω_c and not on the center frequency ω', which is an outstanding advantage compared to filters based on the SOGI.

To investigate the filtering characteristic of the FOCVF without loss of generality, assume that $\omega' = \omega_1 = 100\pi$ (ω_1 is the rated grid frequency in this paper). A bode diagram of this is plotted in Fig. 2.

It can be observed from Fig. 2 that the FOCVF achieves a unity gain and a zero phase at the center frequency. Moreover, the FOCVF can distinguish between 50Hz and -50Hz. It can also be found that a smaller ω_c leads to a better harmonic attenuation. However, the dynamic response becomes very slow at the same time. A tradeoff between the dynamic response and the harmonic attenuation is usually made to determine ω_c under the premise of meeting the system performance requirements. Assume that the performance indexes for a FOCVF are that: 1) the transition time is less than T_p ; 2) the harmonic attenuation ratio for the dominant harmonics is less than $r\%$.

The step response of the FOCVF can be derived from (4) as:

$$c(t) = \frac{\omega_c}{\omega_c - j\omega'}(1 - e^{-\omega_c t}(\cos(\omega' t) + \sin(\omega' t))) \tag{5}$$

It can be seen from (5) that the transition time of $c(t)$ is irrelevant to ω'. Specially, when $\omega' = 0$, $c(t) = 1 - e^{-\omega_c t}$. According to the dynamic response requirement, this can be approximated by:

$$3 \cdot \frac{1}{\omega_c} \le T_p \tag{6}$$

From (1) the harmonic attenuation ratio at the frequency ω is given by $\omega_c \Big/ \sqrt{(\omega - \omega')^2 + \omega_c^2}$. Assume that ω_h is the dominant harmonic nearest ω', according to the harmonic attenuation requirement, there should be:

$$\omega_c \Big/ \sqrt{(\omega_h - \omega')^2 + \omega_c^2} \le r\% \tag{7}$$

By solving (6)-(7), the range of ω_c is obtained as:

$$3/T_p \le \omega_c \le \frac{r\%|\omega_h - \omega'|}{\sqrt{1 - (r\%)^2}} \tag{8}$$

If there is no solution for (3), the HDN or a higher order filter is recommended to replace the FOCVF.

C. FLL

In order to make it accordant for the amplitude and phase of the input signal $\boldsymbol{v}$ and the output signal $\boldsymbol{v}'$, shown in Fig.1a, the center frequency ω' in the FOCVF should be adapted to the input frequency ω of $\boldsymbol{v}$. In this paper, a FLL is proposed to estimate the input frequency ω . Then, the estimated frequency is feed back to the FOCVF as the center frequency.

The combination of the FOCVF and the proposed FLL building blocks is shown in Fig. 3, As can be seen, the FLL has two input signals. One input is the error $\boldsymbol{e}$ of the filter, which is given by:

$$\boldsymbol{e} = \boldsymbol{v} - \boldsymbol{v}' = e_\alpha + j e_\beta \tag{9}$$

The other input signal of the FLL, which is orthogonal to the input signal $\boldsymbol{v}$, is given by:

$$j\boldsymbol{v} = -v_\beta + j v_\alpha \tag{10}$$

The dot product of $\boldsymbol{e}$ by $j\boldsymbol{v}$ is defined as a frequency error variable ε_f :

$$\varepsilon_f = \boldsymbol{e} \cdot (j\boldsymbol{v}) = -e_\alpha v_\beta + e_\beta v_\alpha \tag{11}$$

As a sequence, the FLL controller can be designed as:

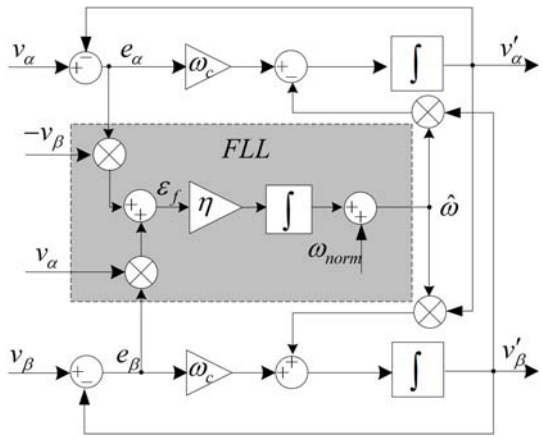

Fig. 3. Structure of the proposed adaptive FOCVF with FLL.

$$\hat{\omega} = \eta \cdot \int \varepsilon_f + \omega_{norm} \tag{12}$$

where $\hat{\omega}$ is the estimated frequency by the FLL, η is the integral coefficient ($\eta > 0$), and ω_{norm} is the normal frequency of the input signal.

D. Stability Analysis of the FLL

To validate the correctness of the proposed FLL, a stability analysis is made for it as follows.

According to (2), the following can be obtained:

$$\begin{cases} \dot{v}_\alpha = -\omega v_\beta \\ \dot{v}_\beta = \omega v_\alpha \end{cases} \tag{13}$$

According to Fig. 2 and (13), the dynamic equation for the filter error $\vec{e}$ can be derived as:

$$\begin{cases} \dot{e}_\alpha = -\omega_c e_\alpha - \hat{\omega} e_\beta - \tilde{\omega} v_\beta \\ \dot{e}_\beta = -\omega_c e_\beta + \hat{\omega} e_\alpha + \tilde{\omega} v_\alpha \end{cases} \tag{14}$$

where $\tilde{\omega} = \omega - \hat{\omega}$.

Actually, the input frequency ω is considered as a constant. From (12), the following can be obtained:

$$\dot{\tilde{\omega}} = -\dot{\hat{\omega}} = -\eta(v_\alpha e_\beta - v_\beta e_\alpha) \tag{15}$$

Thus, (14)-(15) describe the FLL system. Let $\boldsymbol{x} = (x_1, x_2, x_3) = (e_\alpha, e_\beta, \tilde{\omega})$, obviously, $\boldsymbol{x} = 0$ (the origin) is one equilibrium point.

Define a Lyapunov function candidate as:

$$V(x) = 0.5(x_1^2 + x_2^2 + x_3^2/\eta) \tag{16}$$

Let $D = \{x \mid x \in R^3\}$, then $V(x)$ is a positive definite in D. The time derivative of V along the trajectories of the system is given by:

$$\dot{V}(x) = -\omega_c(x_1^2 + x_2^2) \le 0 \tag{17}$$

$\dot{V}(x)$ is negative semi-definite in D. Let $\dot{V}(x) = 0$, so that $x_1, x_2 = 0$. If $x_1, x_2 \equiv 0$, it can be derived from (12) that $x_3 \equiv 0$. Thus, the invariant set $M = \{\boldsymbol{x} = 0\}$. Using the LaSalle's invariant principle, it can be concluded that $\boldsymbol{x} = 0$ is global asymptotically stable.

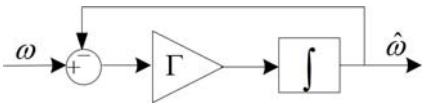

Fig. 4. Linearized FLL system.

E. FLL Tuning

According to (9), (11)-(12), the dynamic equation for $\hat{\omega}$ can be written as:

$$\dot{\hat{\omega}} = \eta(\boldsymbol{v} - \boldsymbol{v}') \cdot (j\boldsymbol{v}) \tag{18}$$

Considering the stable operating conditions, the following relationship between the input and output of the FOCVF is established.

$$\boldsymbol{v}' = \frac{\omega_c}{j(\omega - \hat{\omega}) + \omega_c} \boldsymbol{v} \tag{19}$$

Substituting (19) into (18), yields:

$$\dot{\hat{\omega}} = \eta A^2 \frac{\omega_c(\omega - \hat{\omega})}{(\omega - \hat{\omega})^2 + \omega_c^2} \tag{20}$$

Obviously, this FLL is a nonlinear system. Since the frequency deviation $(\omega - \hat{\omega})$ is very small under stable operating conditions, $(\omega - \hat{\omega})^2$ can be neglected compared with ω_c^2. Hence, (20) can be simplified into:

$$\dot{\hat{\omega}} = \frac{\eta A^2}{\omega_c}(\omega - \hat{\omega}) \tag{21}$$

To obtain the ideal linear FLL model shown in Fig. 4, η can be normalized by:

$$\eta = \Gamma \frac{\omega_c}{A^2} \tag{22}$$

According to Fig. 4, the transfer function of the linearized FLL is given by:

$$\frac{\hat{\omega}}{\omega} = \frac{\Gamma}{s + \Gamma} \tag{23}$$

It can be seen from (23) that the linearized FLL is a first-order inertia element. Thus, the design of the parameter Γ can be approximated by:

$$\Gamma = \frac{3}{t_s} \tag{24}$$

where t_s is the transition time for the step response of the linearized FLL.

III. HDN-FLL

The FOCVF has the ability to extract the FPC from the three-phase grid voltage. However, the performance of the FOCVF with the proposed FLL could be seriously decreased when the grid voltage becomes unbalanced and severely

distorted. On this occasion, it has to set a low cutoff frequency for the FOCVF at the cost of a much slower transient response to voltage variations. However, the accuracy of the FLL does not improve much. In order to overcome the above shortcomings, the HDN structure consisting of multiple adaptive FOCVFs with the FLL, i.e., the HDN-FLL, is presented in this section.

A. HDN Structure

In the $\alpha\beta$ frame, the three-phase grid voltage in terms of the vector is introduced by:

$$\boldsymbol{u}=\frac{2}{3}(u_a+u_b e^{j\frac{2}{3}\pi}+u_c e^{-j\frac{2}{3}\pi})=u_\alpha+ju_\beta \tag{25}$$

Consider the case where grid voltages are unbalanced and distorted by harmonics, $\boldsymbol{u}$ can be expressed as the sum of each harmonic:

$$\boldsymbol{u}=\sum_{-m}^{m}\boldsymbol{u}^i \tag{26}$$

where $-m/m$ denotes the low/upper limit of the harmonic order, and $\boldsymbol{u}^i$ is given by:

$$\begin{aligned}\boldsymbol{u}^i&=\boldsymbol{u}_\alpha^i+j\boldsymbol{u}_\beta^i\\&=V^i\cos(\omega_i t+\varphi_i)+j\sin(\omega_i t+\varphi_i))\end{aligned} \tag{27}$$

where $\omega_i=i\cdot\omega_1$; and i can be a positive or negative integer, which represents $\boldsymbol{v}^i$ is in the positive- or negative-sequence.

The HDN, also called a cross-feedback network, has been widely used as a prefilter for grid synchronization systems in adverse grid voltage conditions. It can accurately extract the fundamental component and interested harmonics from grid voltage. A general HDN structure composed of n ($n=2m+1$) blocks, each containing a FOCVF, is shown in Fig. 5. As can be seen, each output signal, taking $\hat{\boldsymbol{u}}^i$ for instance, is obtained by a FOCVF (tuned at ω_i) filtering the difference between the input $\boldsymbol{u}$ and the cross-feedback signals $\sum\hat{\boldsymbol{u}}^j$ ($j\neq i$). If the structure of the general HDN is stable, $\hat{\boldsymbol{u}}^i$ will converge to the true value $\boldsymbol{u}^i$, while $\hat{\boldsymbol{u}}^j$ converges to $\boldsymbol{u}^j$. However, the stability of general HDN is seldom discussed when n tends to infinite.

B. Stability Analysis of the HDN

As observed from Fig. 5, the HDN can be seen as a set of filters (in dashed box) operating in parallel. Define the filter in dashed box by:

$$G_i(s)=\frac{\hat{\boldsymbol{u}}^i}{\boldsymbol{u}}(s) \tag{28}$$

According to Fig. 5, the following equations can be established:

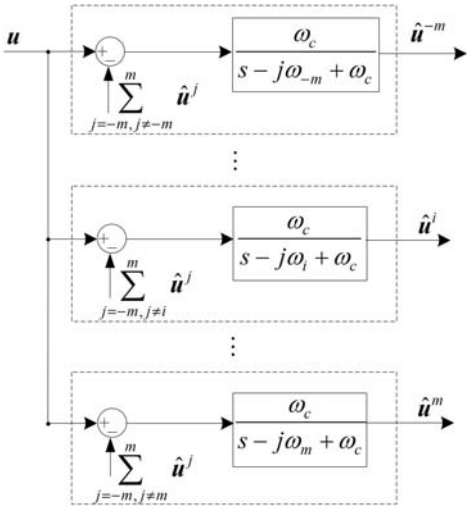

Fig. 5. General HDN composed of *n* blocks

$$\begin{cases}(\boldsymbol{u}-\sum_{j=-m,j\neq -m}^{m}\hat{\boldsymbol{u}}^j)\cdot CV_{(-m)}(s)=\hat{\boldsymbol{u}}^{-m}\\ \quad\vdots\\ (\boldsymbol{u}-\sum_{j=-m,j\neq -i}^{m}\hat{\boldsymbol{u}}^j)\cdot CV_i(s)=\hat{\boldsymbol{u}}^i\\ \quad\vdots\\ (\boldsymbol{u}-\sum_{j=-m,j\neq m}^{m}\hat{\boldsymbol{u}}^j)\cdot CV_m(s)=\hat{\boldsymbol{u}}^m\end{cases} \tag{29}$$

where:

$$CV_i(s)=\frac{\omega_c}{s-j\omega_i+\omega_c} \tag{30}$$

Equation (29) can be expressed in the form of a matrix as:

$$\boldsymbol{u}\begin{bmatrix}1\\ \cdots\\ 1\\ \cdots\\ 1\end{bmatrix}=\boldsymbol{A}\begin{bmatrix}\hat{\boldsymbol{u}}^{(-m)}\\ \cdots\\ \hat{\boldsymbol{u}}^i\\ \cdots\\ \hat{\boldsymbol{u}}^m\end{bmatrix}_{n\times 1} \tag{31}$$

where:

$$\boldsymbol{A}=\begin{bmatrix}\frac{1}{CV_{(-m)}(s)} & \cdots & 1 & 1 & 1\\ \cdots & \cdots & \cdots & 1 & 1\\ 1 & \cdots & \frac{1}{CV_i(s)} & \cdots & 1\\ 1 & 1 & \cdots & \cdots & \cdots\\ 1 & 1 & 1 & \cdots & \frac{1}{CV_m(s)}\end{bmatrix}_{n\times n} \tag{32}$$

Manipulating (31) yields:

$$\begin{bmatrix}\hat{\boldsymbol{u}}^{-m}/\boldsymbol{u}\\ \cdots\\ \hat{\boldsymbol{u}}^i/\boldsymbol{u}\\ \cdots\\ \hat{\boldsymbol{u}}^m/\boldsymbol{u}\end{bmatrix}=\boldsymbol{A}^{-1}\begin{bmatrix}1\\ \cdots\\ 1\\ \cdots\\ 1\end{bmatrix} \tag{33}$$

Substituting (28) into (33), it can be observed that $G_i(s)$ is the sum of the elements in the corresponding row of $\boldsymbol{A}^{-1}$. Thus, $G_i(s)$ can be calculated as:

$$G_i(s)=\frac{CV_i(s)\prod_{j=-m,j\neq i}^{m}(1-CV_j(s))}{\prod_{k=-m}^{m}(1-CV_k(s))+\sum_{k=-m}^{m}(CV_k(s)\prod_{j=-m,j\neq k}^{m}(1-CV_j(s))} \tag{34}$$

By substituting (30) into (34), the following can be obtained:

$$G_i(s)=\frac{\omega_c\prod_{j=-m,j\neq i}^{m}(s-j\omega_j)}{\prod_{k=-m}^{m}(s-j\omega_k)+\omega_c\sum_{k=-m}^{m}(\prod_{j=-m,j\neq k}^{m}(s-j\omega_j))} \tag{35}$$

Equation (35) indicates that the HDN is in essence a *n*-th order complex vector filter. As can be seen in (35), the zero located at ω_j on the imaginary axis means the elimination of the *j*th-component; and the stability of the HDN depends on the locations of poles. If all of the n poles of (35) can be proved to be located in the left half plane, the HDN is stable. To that end, it can be observed from the feature of the denominator that the eigenvalues of $G_i(s)$ is suitable to be analyzed by the root locus method.

The characteristic equation of $G_i(s)$ is given by:

$$\prod_{k=-m}^{m}(s-j\omega_k)+\omega_c\sum_{k=-m}^{m}(\prod_{j=-m,j\neq k}^{m}(s-j\omega_j))=0 \tag{36}$$

Let $\omega_c=0$. Then, (36) can be manipulated into:

$$\prod_{k=-m}^{m}(s-j\omega_k)=\prod_{i=1}^{n}(s-p_i)=0 \tag{37}$$

where $p_i=j\omega_k$ is the starting point of a root locus branch.

Then, let $\omega_c\to+\infty$, and (36) can be manipulated into:

$$\sum_{k=-m}^{m}(\prod_{j=-m,j\neq k}^{m}(s-j\omega_j))=\prod_{i=1}^{n-1}(s-z_i)=0 \tag{38}$$

where z_i is the ending point of a root locus branch.

Obviously, for any $i\in[-m,m]$, $s=j\omega_i$ is not a root of (38). Dividing the first term of (38) by $\prod_{i=-m}^{m}(s-j\omega_i)$ yields:

$$\sum_{i=-m}^{m}\frac{1}{s-j\omega_i}=0 \tag{39}$$

It can be simply verified that $s=j\omega_i'$ is a root of (39), while ω_i' meets the following constraint condition:

$$\omega_i<\omega_i'<\omega_{i+1} \tag{40}$$

Thus, it is possible to make $z_i=j\omega_i'$.

The only asymptote equation is given by:

$$j\omega=\sum_{i=1}^{n}p_i-\sum_{i=1}^{n-1}z_i \tag{41}$$

According to the principle of the phase-angle condition, the starting angle at p_i, denoted by θ_{pi}, and the ending angle at z_i, denoted by φ_{zi}, can be calculated as:

$$\theta_{pi}=(2k+1)\pi+\sum_{j=1}^{n-1}\varphi_{z_jp_i}-\sum_{j=1,j\neq i}^{n}\theta_{p_jp_i}=\pi \tag{42}$$

and:

$$\varphi_{zi}=(2k+1)\pi-\sum_{j=1,j\neq i}^{n-1}\varphi_{z_jz_i}+\sum_{j=1}^{n}\theta_{p_jz_i}=\pi \tag{43}$$

respectively, where φ_{ab} or θ_{ab} denotes the angle from point a to b ($a,b\in\{z_i,p_i\}$).

After that, the root locus of $G_i(s)$ is plotted in Fig. 6. It can be observed that the n branches of the root locus are all located in the left half plane as long as $\omega_c>0$. Hence, the stability of the general HDN is verified. In addition, to ensure a better dynamic performance, ω_c cannot be set too small or too large, both of which lead the roots close to the imaginary axis. To determine the range of ω_c for a practical application, to achieve the best dynamic response, some mathematical software tools like "Matlab" can be used, and the specific steps are given as follows.

A custom HDN consisting of a limited number of blocks, (34) could be rewritten as:

$$\sum_{k\in G}(s-\omega_k)^{-1}+\frac{1}{\omega_c}=0 \tag{44}$$

where *G* is the set of selected harmonics to be exacted by HDN, such as $G=\{1,-1,-5,7\}$.

It is convenient to solve (44) with the Matlab program, with ω_c in increments of a fixed-step (such as 10π) from 0 to a proper upper limit. Assuming that s_i is the dominant pole for (44), the best ω_c would be found when $real(s_i)$ reaches the minimum value. For example, in the case of $G=\{1,-1,-5,7\}$ or $G=\{1,-1,-5,7,-11,13\}$, the range of the optimal ω_c can be determined to be $[80\pi,90\pi]$ by following the above steps.

C. HDN-FLL

Applying the adaptive FOCVF with the proposed FLL to the HDN, the HDN-FLL structure for gird synchronization is

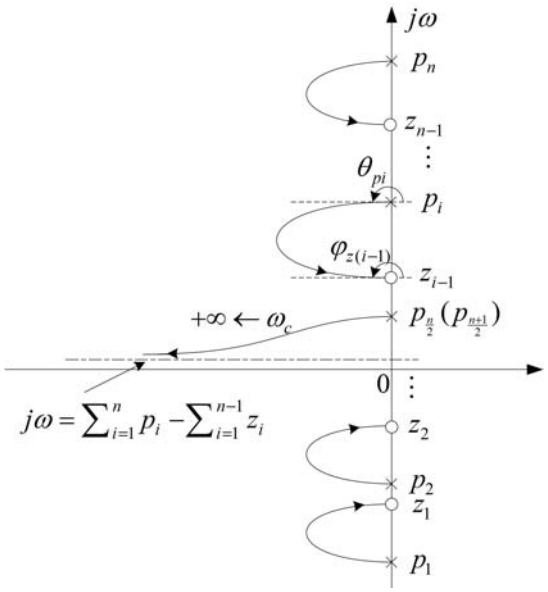

Fig. 6. Root locus of $G_i(s)$

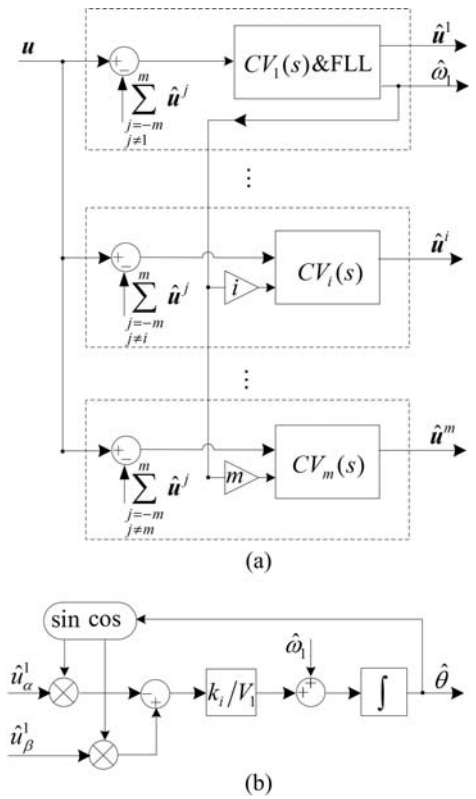

Fig. 7. Block diagram of HDN-FLL synchronization method ((a) grid frequency estimation and harmonic detection and (b) grid phase estimation).

achieved, which is graphically represented in Fig. 7. As can be seen, the grid frequency is estimated by the FLL, then multiplied by the harmonic order to be feedback to each of the FOCVFs to make them frequency adaptive. Thus, each frequency component can be accurately exacted even in the case of grid frequency fluctuations.

It is also important to extract the gird phase information for grid synchronization. Let θ be the grid phase, and $\theta = \omega_1 t + \varphi_1$. $\hat{\theta}$ is the estimation of θ, and $\hat{\theta} = \hat{\omega}_1 t + \hat{\varphi}_1$. Due to the action of the FLL, it is reasonable to assume that $\hat{\omega}_1 = \omega_1$, hence:

$$\theta - \hat{\theta} = \varphi_1 - \hat{\varphi}_1 = \triangle\varphi \tag{45}$$

When $\triangle\varphi$ is small, $\triangle\varphi \approx \sin\triangle\varphi$. Therefore, the estimator of the grid phase can be designed as:

$$\hat{\theta}_1 = \int(\hat{\omega}_1 + k_i \cdot \triangle\varphi)dt = \int(\hat{\omega}_1 + k_i \cdot \sin\triangle\varphi)dt \tag{46}$$

Due to the presence of the HDN, it can be considered that $\hat{\boldsymbol{u}}^1 \approx \boldsymbol{u}^1 = V_1(\cos\theta + j\sin\theta)$. Therefore, $\sin\triangle\varphi$ can be calculated by:

$$\sin\triangle\varphi = (\hat{u}^1_\beta \cos\hat{\theta} - \hat{u}^1_\alpha \sin\hat{\theta})/V_1 \tag{47}$$

where $V_1 = \sqrt{(\hat{u}^1_\alpha)^2 + (\hat{u}^1_\beta)^2}$.

Finally, a block diagram of the gird phase estimation is depicted in Fig. 7(b).

IV. Simulation Results

In order to evaluate the performance of the HDN-FLL shown in Fig. 7, a series of simulations are carried out under several adverse grid conditions. Simultaneously, to highlight the advantages of the proposed FLL, the HDN-FLL is compared with the Multiple-Complex Coefficient Filter (MCCF) method in [12], which is a PLL-type synchronization technique based on the structure of the HDN and has the same functions as the former. In this section, the HDN is made up of 4 blocks corresponding to 1^{th}, -1^{th}, -5^{th}, 7^{th} harmonic extraction, respectively. The control parameters for the HDN-FLL are set as: the cutoff frequency $\omega_c = 80\pi$, and the FLL controller gain $\eta = 0.3$. To get those for the MCCF refer to [12].

Fig. 8 shows the input three-phase voltage signal of the simulation tests. The amplitude and frequency of the pre-fault voltage are set to 311V and 50 Hz, respectively. A voltage fault occurs at 0.2s and continues until the end of the simulation time, which causes the grid voltage to become unbalanced and distorted. In addition, the parameters of the fault voltage refer to Table I. At 0.4s, the grid frequency is suddenly varied from 50 Hz to 45 Hz and continues that for the rest of the simulation time. At 0.6s, the grid phase-angle is jumped by 38 degree.

Fig. 9 and Fig. 10 show the responses of the HDN-FLL and the MCCF to the input voltage signal, respectively. As can be seen, both the HDN-FLL and the MCCF have zero error estimations of the grid frequency, phase and magnitudes of the harmonics in the steady state, which verifies the excellent steady-state performance of both methods. In attrition, their performance differences mainly lie in the transient responses.

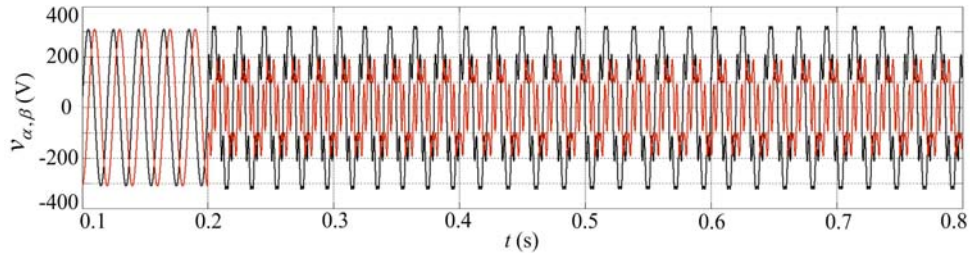

Fig. 8. Input three-phase grid voltage signal.

TABLE I
PARAMETERS OF FAULT INPUT VOLTAGE

Harmonic order	Value [V]
+1	$220\angle 0^{\circ}$
-1	$80\angle 0^{\circ}$
-5	$70\angle 0^{\circ}$
+7	$60\angle 0^{\circ}$

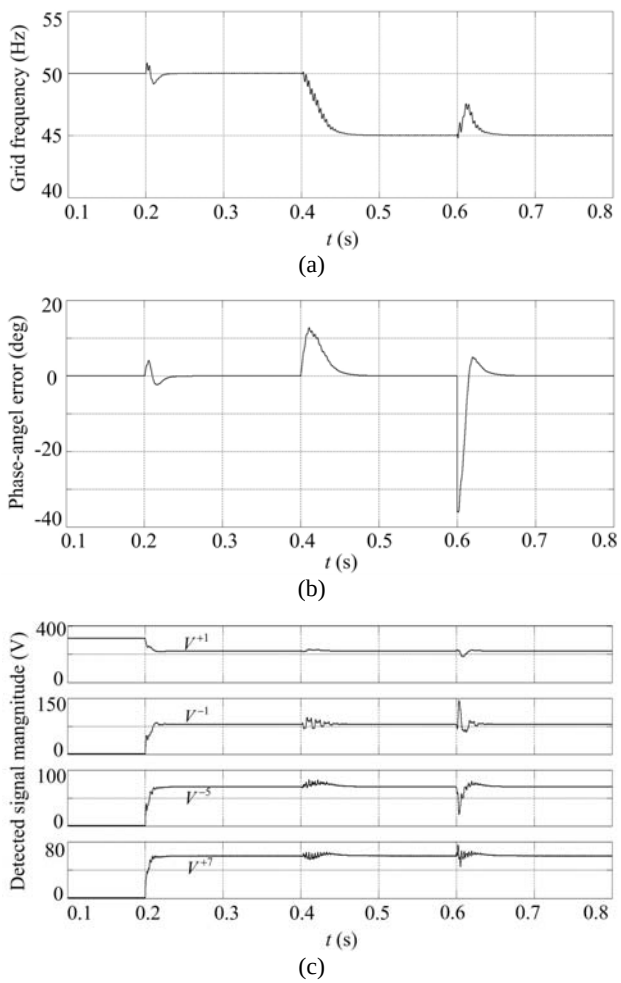

Fig. 9. Simulation results of the response for HDN-FLL ((a) estimated grid frequency, (b) error between the actual and estimated grid phase, and (c) detected magnitudes of harmonics).

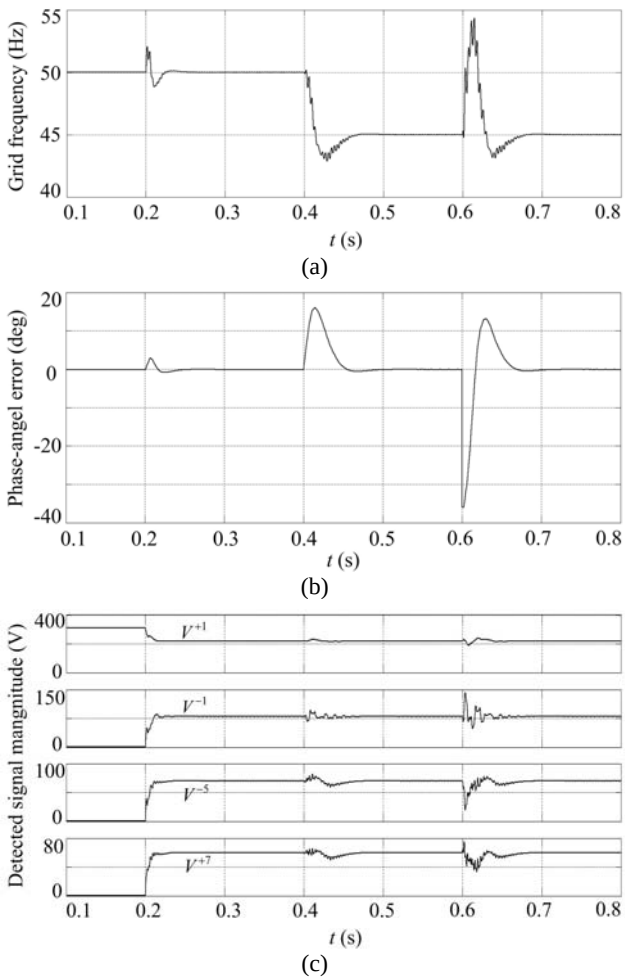

Fig. 10. Simulation results of the response for MCCF ((a) estimated grid frequency, (b) error between the actual and estimated grid phase, and (c) detected magnitudes of harmonics).

For the grid frequency estimation, in the transient processes after times 0.2 s, 0.4 s, and 0.6 s, it can be seen that the HDN-FLL has shorter transient times and smaller overshoot when compared with the MCCF, which is particularly evident when the phase-angle jump occurs. In this case, the HDN-FLL has a transient time of 40 ms and an overshoot of 5.5%, while those for the MCCF are 70ms and 20.1%, respectively.

For the grid phase estimation, the HDN-FLL has a smaller overshoot than the MCCF in the case of a frequency

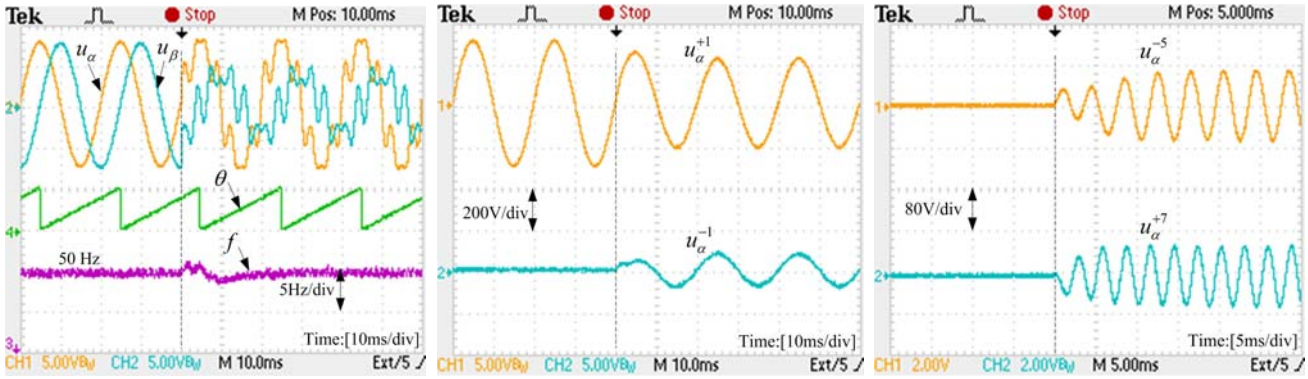

(a) (b) (c)

Fig. 11. Experimental results of test case 1 ((a) input grid voltages, estimated phase-angel and frequency, (b) detected fundamental positive- and negative- sequence, and (c) detected 5th and 7th harmonics).

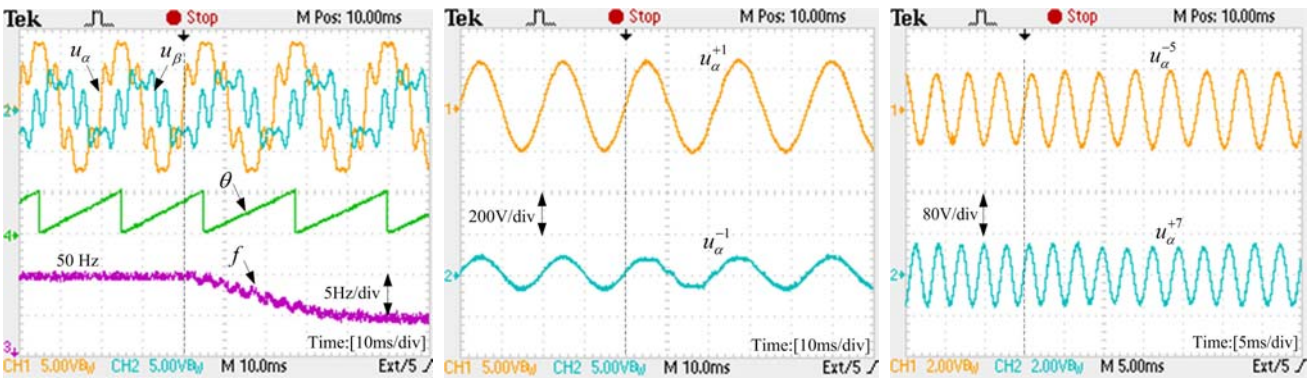

(a) (b) (c)

Fig. 12. Experimental results of test case 2 ((a) input grid voltages, estimated grid phase and frequency, (b) detected fundamental positive- and negative- sequence, and (c) detected 5th and 7th harmonics).

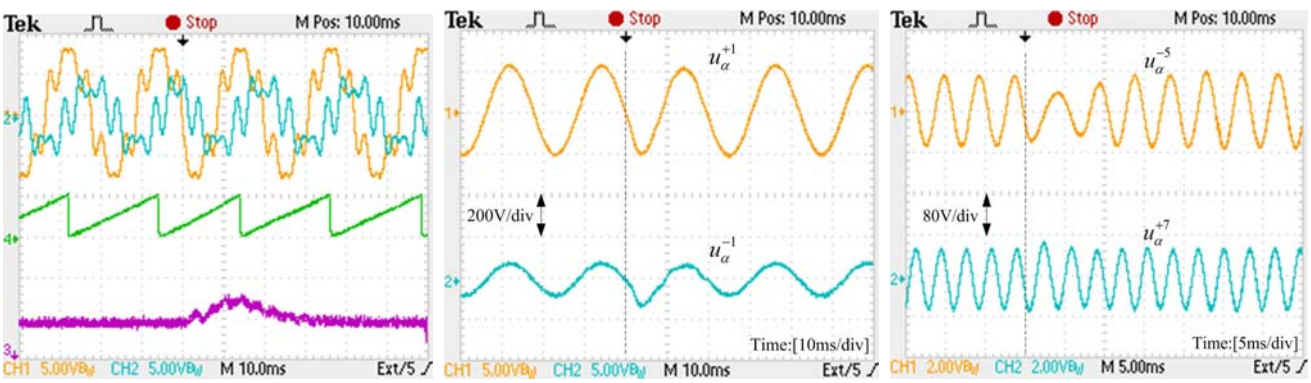

(a) (b) (c)

Fig. 13. Experimental results of test case 3 ((a) input grid voltages, estimated grid phase and frequency, (b) detected fundamental positive- and negative- sequence, and (c) detected 5th and 7th harmonic).

fluctuation or phase-angle jump.

For harmonic detection, due to having a faster frequency estimation with a smaller fluctuation, the HDN-FLL is expected to have better dynamic performance than the MCCF in this respect, and this is confirmed by the contrast simulation results as well. Most significantly of all, it can be seen that the HDN-FLL has a much shorter and smoother transient than the MCCF in the case of a phase-angle jump.

Based on the above comparative analysis, it can be concluded that the HDN-FLL does a better job than the MCCF in the transient response to phase-angle jumps or frequency shift under unbalanced and distorted grid conditions.

V. Experimental Results

The algorithm of the HDN-FLL is implemented in the control board based on a TMS320F28335 which is a

floating-point 32-bit 150-MHz DSP. The input three-phase grid voltage used in the experiments is simulated by a waveform generator program based on a DSP. Moreover, the sampling rate is 20 kHz. A 12-bit 4-channel digital-to-analog converter (DAC) is used to display the signals in a digital oscilloscope.

Three test cases are designed to experimentally validate the HDN-FLL under adverse grid conditions, which are consistent with the simulation study.

1) Test case 1: An ideal three-phase grid voltage (amplitude of 311 V) becomes unbalanced and distorted when a voltage fault occurs, with a constant frequency of 50 Hz. The parameters of the fault voltage are the same as those listed in Table I.

2) Test case 2: The frequency of the fault voltage varies from 50 Hz to 45 Hz.

3) Test case 3: The phase-angle of the fault voltage (45 Hz) jumps by 38 degrees.

The experimental results of test cases 1-3 are depicted in Figs. 11-13, respectively. The input gird voltages u_α and u_β, the estimated gird frequency f, and the phase–angle θ are shown together. For the sake of clarity, only the components on the α-axle of the detected 1th, -1th, -5th and 7th harmonics are shown, which are denoted by u_α^{+1}, u_α^{-1}, u_α^{-5} and u_α^{+7}, respectively. Since the harmonics have very short periods, (u_α^{+1}, u_α^{-1}) and (u_α^{-5}, u_α^{+7}) are presented in different time scales, respectively.

As seen in Fig. 11 (Test case 1), the HDN-FLL can operate satisfactorily under both norm and fault grid voltages. The grid frequency and phase angle can be estimated precisely. The 1th, -1th, -5th and 7th harmonics can also be accurately exacted, with the amplitudes of the waveforms equal to the preset values in Table I. Moreover, the HDN-FLL system undergoes a transient of about 15 ms after the voltage fault occurs. During this period of time, the estimated frequency f fluctuates slightly with a ripple less than 2 Hz.

In Fig. 12 (Test case 2), the HDN-FLL system undergoes a longer transient of about 40 ms after the 5 Hz frequency shift occurs. After that, the HDN-FLL gives a precise estimate of the grid frequency, phase-angle and harmonics at the new frequency.

In Fig. 13 (Test case 3), the system undergoes a transient of 30 ms after the phase jump occurs. The estimated frequency f fluctuates with a ripple of no more than 3 Hz. In addition, all of the estimated variables achieve the desired values.

From the above experimental results, it can be concluded that the HDN-FLL can operate well and has excellent grid synchronization and harmonics detection functions under unbalanced and distorted grid voltage conditions, even when a frequency shift and a phase jump are present simultaneously.

VI. Conclusions

In this paper, a grid synchronization technique called HDN-FLL has been proposed, and its stability has been verified. Simulations are conducted to compare the proposed method with the MCCF. Experimental results verify the effectiveness of the HDN-FLL. The following conclusions are recognized. 1) the HDN-FLL can achieve fast and exact estimation of the gird frequency and phase-angle under unbalanced and distorted grid voltage conditions; 2) the HDN-FLL can extract the FPC, the FNC and other interested harmonics from the grid voltage with no interference to or from the others; 3) compared with the MCCF, the HDN-FLL has better dynamic performance in the case of phase-angle jumps, which chiefly shows a shorter transient time and a smaller ripple in frequency estimation. These features make the HDN-FLL attractive for the grid-interfaced converters in distributed generation systems under adverse gird conditions, since they enable the grid-interfaced converters to be multifunctional, such as selective harmonic compensation, power quality monitoring, islanding detection, and so on.

Acknowledgment

This work was supported by the National Natural Science Foundation of China under Grant 61203031, the National High-tech R&D Program of China under Grant 2015AA050604, the Project of Innovation-driven Plan in Central South University, and Hunan province science and technology plan under Grant 2013GK3001.

References

[1] J. M. Carrasco, L. G. Franquelo, J. T. Bialasiewicz, and E. Galvan, “Power electronic systems for the grid integration of renewable energy sources: a survey,” *IEEE Trans. Ind. Electron*., Vol. 53, No. 4, pp. 1002-1016, Jun. 2006.

[2] F. M. Hughes, O. Anaya-Lara, N. Jenkins, and G. Strbac, “Control of DFIG-based wind generation for power network support,” *IEEE Trans. Power Syst.*, Vol. 20, No. 4, pp. 1958–1966, Nov. 2005.

[3] W. Sinsukthavorn, E. Ortjohann, A. Mohd, N. Hamsic, and D. Morton, “Control strategy for three-/four-wire inverter-based distributed generation,” *IEEE Trans. Ind. Electron.*, Vol. 59, No. 10, pp. 3890–3899, Oct. 2012.

[4] A. Kahrobaeian and Y. A. R. I. Mohamed, “Networked-based hybrid distributed power sharing and control for islanded microgrid systems,” *IEEE Trans. Power Electron.*, Vol. 30, No. 2, pp.603-617, Feb. 2015.

[5] F. Blaabjerg, R. Teodorescu, M. Liserre, and A. V. Timbus, “Overview of control and grid synchronization for distributed power generation systems,” *IEEE Trans. Ind. Electron*., Vol. 53, No. 5, pp. 1398-1409, Oct. 2006.

[6] M. Altýn, O. Gooksu, R. Teodorescu, and P. Rodriguez, “Overview of recent grid codes for wind power integration,” in *12th International Conference on OPTIM*, pp. 1152–1160, 2010.

[7] M. Tsili and S. Papathanassiou, "A review of grid code technical requirements for wind farms," *IET Renewable Power Generation*, Vol. 3, No. 3, pp. 308–332, Sep. 2009.
[8] J. He, Y. W. Li, and S. Munir, "A flexible harmonic control approach through voltage controlled DG-grid interfacing converters," *IEEE Trans. Ind. Electron*., Vol. 59, No. 1, pp. 444–455, Jan. 2012.
[9] P. Rodriguez, J. Pou, J. Bergas, and J. I. Candela, "Decoupled double synchronous reference frame PLL for power converters control," *IEEE Trans. Power Electron*., Vol. 22, No. 2, pp. 584–592, Mar. 2007.
[10] P. Rodriguez, R. Teodorescu, and I. Candela, "New positive-sequence voltage detector for grid synchronization of power converters under faulty grid conditions," in *37th IEEE Power Electronics Specialists Conference*, pp. 1-7, Jun. 2006.
[11] P. Rodriguez, A. Luna, I. Candela, R. Mujal, R. Teodorescu, and F. Blaabjerg, "Multiresonant frequency-locked loop for grid synchronization of power converters under distorted grid conditions," *IEEE Trans. Ind. Electron*., Vol. 58, No. 1, pp. 127–138, Jan. 2011.
[12] X. Guo, W. Wu, and Z. Chen, "Multiple-complex coefficient-filter-based phase-locked loop and synchronization technique for three-phase grid interfaced converters in distributed utility networks," *IEEE Trans. Ind. Electron*., Vol. 58, No. 4, pp. 1194–1204, Apr. 2011.
[13] X. Q. Guo and W. Y. Wu, "Simple synchronisation technique for three-phase grid-connected distributed generation systems," *IET Renewable Power Generation*, Vol. 7, No.1, pp. 55-62, Feb. 2013.
[14] W. W. Li, X. B. Ruan, C. L. Bao, D. H. Pan, and X. H. Wang, "Grid synchronization systems of three-phase grid-connected power converters: a complex vector filter perspective," *IEEE Trans. Ind. Electron.*, Vol. 61, No. 4, pp. 1855-1870, Apr. 2014.
[15] X. Du, Y. D. Liu, G. N. Wang, and P. J. Sun, "Three-phase grid voltage synchronization using sinusoidal amplitude integrator in synchronous reference frame," *International Journal of Electrical Power & Energy Systems*, Vol. 64, pp. 861-872, Jan. 2015.
[16] Y. F. Wang and Y. W. Li, "Grid synchronization PLL based on cascaded delayed signal cancellation," *IEEE Trans. Power Electron*., Vol. 26, No. 7, pp. 1987–1997, Jul. 2011.
[17] K. J. Lee, D. S. Shin, H. J. Kim, J. P. Lee, T. J. Kim, and D. W. Yoo, "Phase-locked loop algorithm using FFT concept for grid synchronization under unbalanced voltage sags," in *28th Annual IEEE Applied Power Electronics Conference and Exposition (APEC)*, pp. 2231-2234, Mar. 2013.
[18] K. J. Lee, J. P. Lee, D. S. Shin, D. W. Yoo, and H. J. Kim, "A novel grid synchronization PLL method based on adaptive low-pass notch filter for grid-connected PCS," *IEEE Trans. Ind. Electron*., Vol. 61, No. 1, pp. 292-301, Jan. 2014.
[19] M. Karimi-Ghartemani and M. R. Iravani, "A method for synchronization of power electronic converters in polluted and variable-frequency environments," *IEEE Trans. Power Syst*., Vol. 19, No. 3, pp. 1263–1270, Aug. 2004.
[20] D. Yazdani, A. Bakhshai, G. Joos, and M. Mojiri, "A nonlinear adaptive synchronization technique for grid-connected distributed energy sources," *IEEE Trans. Power Electron*., Vol. 23, No. 4, pp. 2181–2186, Jul. 2008.
[21] X. Yuan, W. Merk, H. Stemmler, and J. Allmeling, "Stationary frame generalized integrators for current control of active power filters with zero steady-state error for current harmonics of concern under unbalanced and distorted operating conditions," *IEEE Trans. Ind. Appl*., Vol. 38, No. 2, pp. 523–532, Mar./Apr. 2002.
[22] M. Ciobotaru, R. Teodorescu, and F. Blaabjerg, "A new single-phase PLL structure based on second order generalized integrator," in *Proceedings of IEEE PESC*, pp. 1–7, 2006.
[23] P. Rodriguez, A. Luna, I. Candela, R. Teodorescu, and F. Blaabjerg, "Grid synchronization of power converters using multiple second order generalized integrators," in *34th Annual Conference of IEEE Industrial Electronics*, pp. 755–760, Nov. 2008.
[24] P. Rodriguez, A. Luna, M. Ciobotaru, R. Teodorescu, and F. Blaabjerg, "Advanced grid synchronization system for power converters under unbalanced and distorted operating conditions," in *32nd Annual Conference on IEEE Industrial Electronics*, pp. 5173–5178, Nov. 2006.

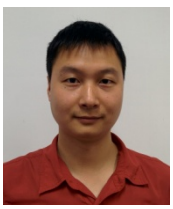

Zhaoxu Luo was born in China, in 1987. He received his B.S. and M.S. degrees from Central South University, Changsha, China, in 2008 and 2011, respectively; where he is presently a Ph.D. candidate. His current research interests include power electronics technology and power quality control.

Mei Su was born in China, in 1967. She received her B.S., M.S. and Ph.D. degrees from the School of Information Science and Engineering, Central South University, Changsha, China, in 1989, 1992 and 2005, respectively. Since 2006, she has been a Professor in the School of Information Science and Engineering, Central South University. Her current research interests include matrix converters and wind energy conversion systems.

Yao Sun was born in China, in 1981. He received his B.S., M.S. and Ph.D. degrees from the School of Information Science and Engineering, Central South University, Changsha, China, in 2004, 2007 and 2010, respectively. He is presently an Associate Professor in the School of Information Science and Engineering, Central South University. His current research interests include matrix converters, micro-grids and wind energy conversion systems.

Zhangjie Liu was born in China, in 1991. He received his B.S. degree in Detection Guidance and Control Techniques from the Central South University, Changsha, China, in 2013; where he is presently working towards his Ph.D. degree in Control Engineering. His current research interests include renewable energy systems, distributed generation and DC micro-grids.

Mi Dong was born in China, in 1976. She received her B.S., M.S. and Ph.D. degrees from the School of Information Science and Engineering, Central South University, Changsha, China, in 1994, 2002 and 2007, respectively. She is presently an Associate Professor in the School of Information Science and Engineering, Central South University. Her current research interests include photovoltaic power technology, micro-grids, and power quality control.